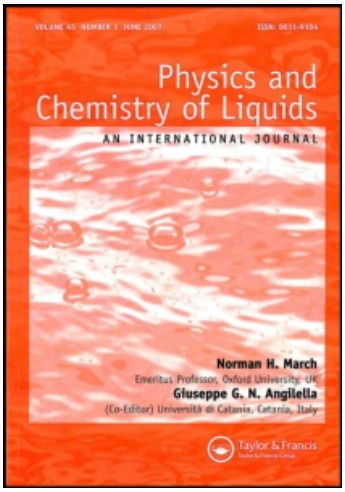

Physics and Chemistry of Liquids
Publication details, including instructions for authors and subscription information:
http://www.informaworld.com/smpp/title~content=t713646857

Structural transitions in interionic force models of liquid $AlCl_3$

R. Ruberto[a]; G. Pastore[bc]; M. P. Tosi[d]
[a] CNISM and Dipartimento di Fisica dell'Università, I-98166 Messina, Italy [b] Dipartimento di Fisica Teorica dell'Università, I-34100 Trieste, Italy [c] CNR-INFM DEMOCRITOS National Simulation Center, I-34100 Trieste, Italy [d] NEST-CNR-INFM and Scuola Normale Superiore, I-56126 Pisa, Italy

To cite this Article Ruberto, R. , Pastore, G. and Tosi, M. P.(2008) 'Structural transitions in interionic force models of liquid $AlCl_3$', Physics and Chemistry of Liquids, 46: 5, 548 — 563
To link to this Article: DOI: 10.1080/00319100801932371
URL: http://dx.doi.org/10.1080/00319100801932371

Physics and Chemistry of Liquids
Vol. 46, No. 5, October 2008, 548–563

Taylor & Francis
Taylor & Francis Group

Structural transitions in interionic force models of liquid $AlCl_3$

R. Ruberto[a], G. Pastore[bc]* and M.P. Tosi[d]

[a]*CNISM and Dipartimento di Fisica dell'Università, I-98166 Messina, Italy;* [b]*Dipartimento di Fisica Teorica dell'Università, I-34100 Trieste, Italy;* [c]*CNR-INFM DEMOCRITOS National Simulation Center, I-34100 Trieste, Italy;* [d]*NEST-CNR-INFM and Scuola Normale Superiore, I-56126 Pisa, Italy*

(*Received 21 January 2008; final version received 21 January 2008*)

We present molecular dynamics simulation of an interionic force model of liquid $AlCl_3$ along a few paths in the temperature-density plane. These paths include (1) an isobar and an isochore starting from the experimental standard freezing point (SFP), and (2) high-temperature isotherms starting from the isochore passing through the SFP. Our calculations show: the dissociation of dimers and higher molecular clusters into monomers with increasing temperature both along the experimental atmospheric pressure isobar and along the SFP isochore; and the pressure-induced molecular-to-ionic (MI) transition accompanied by, or followed by, solidification on increasing density along the two isotherms. The high-pressure solid structure is of the same layer type, with 6-fold coordinated metal ions, met at standard pressure. Crossing of the mean square displacements of the two ionic species provides a clear signal of the MI transition in the liquid. We discuss the consistency of our results with recent X-ray diffraction experiments on $AlCl_3$ under pressure.

Keywords: molten salts; molecular liquids; pressure induced transitions; polarisable models

1. Introduction

The unusual melting process of $AlCl_3$ has drawn much attention to the structure of the melt near the standard freezing point (SFP) (for a review on trihalides, refer to the study by Tosi *et al*. [1]). At atmospheric pressure the material melts from an ionic layer structure with 6-fold coordination of the Al ions [2] into a 4-fold coordinated liquid showing macroscopic properties that are typical of molecular liquids (in particular, very low ionic conductivity combined with low viscosity [3]). Neutron diffraction experiments [4] have confirmed the tetrahedral-like coordination of Al in the melt, that was first reported from X-ray diffraction experiments [5], and have shown that the neutron-weighted liquid structure factor of $AlCl_3$ is topologically very similar to that of $AlBr_3$ and $GaBr_3$ [6], which melts into molecular liquid from a crystal structure formed from dimeric molecular units [2]. The $AlCl_3$ melt has also been described as made of disordered fragments of a tetrahedral network with a large number of microvoids [7]. Theoretical studies of the liquid structure at the experimental SFP have been based both on *ab initio* approaches [8,9] and on pseudo-classical interionic force models [10,11], and their results are overall in good

*Corresponding author. Email: pastore@ts.infn.it

ISSN 0031–9104 print/ISSN 1029–0451 online

DOI: 10.1080/00319100801932371
http://www.informaworld.com

agreement with the neutron diffraction data. In particular, it was shown [11] that upon inclusion of van der Waals Cl–Cl interactions, one obtains quantitative agreement with the first sharp diffraction peak in the observed neutron-weighted structure factor [4]. As is well known, this structural feature gives a clear signal of intermediate range order. An analysis of cluster populations in the melt by the same model [12] has shown that a majority of recognisable dimers is present at the SFP together with several types of higher clusters, including trimers of a chain-like type that can be viewed as formed by attaching a monomer to a dimer via edge sharing. The same trimer is met in *ab initio* calculations on isolated clusters [8,9].

Brazhkin *et al*. [13,14] have recently reported experimental X-ray diffraction studies of $AlCl_3$ extending away from the SFP up to high temperature and pressure. These authors have followed the melting curve up to about 1400°C and 6 GPa and have reported (1) a breakdown of the intermediate range order in the melt with increasing pressure, followed by (2) a rather abrupt change in the slope of the melting curve. The latter feature is interpreted as a signal that the molecular-to-ionic (MI) transition is branching out from the melting curve to become a liquid–liquid transition. The MI transition in this liquid is due, of course, to the breakage of a network of molecular clusters into a liquid of dissociated ions, without a substantial change in the electronic structure of the ions. Nevertheless this behaviour as displayed by a classical liquid brought to extreme thermodynamic conditions is reminiscent of the prototypic scenario provided by molecular hydrogen for molecular dissociation and pressure ionisation occurring under isochoric heating [15,16].

In the present work we use the interionic force model adopted by Ruberto *et al*. [11] for liquid $AlCl_3$ at the SFP to explore by classical molecular dynamic simulations the structural transitions that occur along extended paths in the temperature-density (T, ρ) plane. The results demonstrate dissociation of higher clusters into monomers on increasing temperature along the isochore passing through the experimental SFP, and breakage of molecular clusters accompanied by, or followed by, solidification on increasing density along two isotherms starting from high-temperature points on the above isochore. The model ionic interactions are constructed from Born–Mayer type pair potentials supplemented by shell model dipoles located on the halogens, and involve parameters that were determined in a systematic study of the binding and the vibrational frequencies of monomeric and dimeric units of Al, Fe and Ga chlorides, bromides and iodides [17]. The shell model inclusion of ion core polarisation resulting on the halogen ions from both electrical induction and overlap deformability is indeed crucial to quantitatively emulate chemical bonding in binary ionic systems [18]. Such well-tuned model calculations, although less quantitatively reliable than those based on an *ab initio* approach, allow fast and extensive explorations at low computational cost, and indicate in a direct way the physical mechanisms that lie behind the observed behaviours and what may be the signals to be looked for in *ab initio* or experimental studies. In this sense the present approach can be viewed as complementary to *ab initio* calculations, and indeed hybrid techniques of computer simulation of condensed phases have been proposed that combine in a symbiotic way model interactions and *ab initio* methods [19,20].

Even though the parameters of the interaction model we use have been derived from structural and vibrational data of small clusters, thermodynamic quantities are fairly well reproduced. Indeed, the value of the pressure in our model at the temperature and density of the experimental SFP is about −40 MPa – an error comparable to many other model simulations error [10]. Notwithstanding such an agreement at the SFP, due to the nature

of effective interaction of the model, we decided to adopt the density *in lieu* of the pressure as an independent thermodynamic variable. However, we provide the corresponding values of the pressure within the present model, in order to make contact between our results and the experimental observations of Brazhkin *et al*. [13,14].

The plan of the article is briefly as follows. The essential aspects of the model and of the microcanonical molecular dynamics method are recalled in Section 2, which also describes our choice of simulation paths in the (T, ρ) plane. Section 3 reports our main results for the thermal dissociation of clusters, while Section 4 gives results on the MI liquid–liquid transition and on solidification. Section 5 reports results regarding velocity autocorrelations and mean square ionic displacements leading to diffusion coefficients in the (T, ρ) plane. The article ends in Section 6 with a summary and some discussion of future perspectives.

2. Interionic force law, simulation procedure and road map

We write the potential energy $U(\{\mathbf{r}_{ij}\},\{\mathbf{p}_i\})$ of the liquid simulation sample, which depends on all interionic bond vectors $\mathbf{r}_{ij}$ and all electronic dipoles $\mathbf{p}_i$ carried by the halogens, as

$$U(\{\mathbf{r}_{ij}\},\{\mathbf{p}_i\}) = \sum_{i<j}\left[\frac{z_i z_j e^2}{r_{ij}} + \Phi_{ij}(r_{ij}) - \frac{C_i C_j}{r_{ij}^6}\left(1 - e^{-(r_{ij}/\xi)^6}\right)\right] + U_{\mathrm{pol}}^{\mathrm{cl}}(\{\mathbf{r}_{ij}\},\{\mathbf{p}_i\}) + U_{\mathrm{shell}}(\{\mathbf{r}_{ij}\},\{\mathbf{p}_i\}). \quad (1)$$

The sum in Equation (1) includes: (1) the Coulomb energy of the ionic point charges having nominal valences z_i, (2) the overlap repulsive energy as described by the Busing form [21]

$$\Phi_{ij}(r) = f(\rho_i + \rho_j)\exp\left[\frac{(R_i + R_j - r)}{(\rho_i + \rho_j)}\right] \quad (2)$$

in terms of transferable radii R_i and stiffness parameters ρ_i and (3) the van der Waals interaction energy of the halogens. In regard to the latter, we have avoided the risk of system collapse during a simulation run from the imbalance between inverse sixth power attractions and exponential repulsions in close collisions by the expedient of inserting a continuous saturation factor involving a parameter x. The precise value of this parameter is irrelevant within a range lying between the Al–Cl and Cl–Cl bond lengths ($x \approx 0.2$–0.3 nm).

The electronic polarisation of the halogens is allowed in Equation (1) through both the classical electrical polarisation energy $U_{\mathrm{pol}}^{\mathrm{cl}}$ and the shell deformation energy U_{shell}, the latter being patterned after the shell model used in the lattice dynamics of ionic and semi-conducting crystals [22]. Explicit expressions for these energy terms can be found in study by Akdeniz and Tosi [23]. Saturation of van der Waals attractions at short range as included in Equation (1) is consistent with the saturation of the effective ionic polarisability that is embodied in the shell model. As already noted, we have taken the values of the various force law parameters from the analysis of isolated molecular structures [17].

With the potential energy of the ionic assembly written as a function of the bond vectors and of the dipoles on the halogens, we perform standard microcanonical molecular dynamics calculation using Beeman's algorithm [24]. Our code implements a full

calculation of Ewald sums for all long-range interactions and determines by energy minimisation at each time step of 2 fs the equilibrium values of the dipole moments carried by the chlorines, allowing full control on the accuracy in the evaluation of energy and forces. The details of the simulation protocol regarding initialisation and equilibration of the sample and the subsequent collection of statistics on various sample properties have been described in detail elsewhere [11].

The various symbols in Figure 1 show the position of the thermodynamic states in the (T, ρ) plane for which we have run simulations of the model. Starting from the experimental SFP marked by a crossed circle at $T = 473$ K and $\rho = 1.27\,\mathrm{g\,cm^{-3}}$, we proceed along an extrapolation of the observed temperature–density relation at atmospheric pressure from data by Janz [25] [path (1)] and along the isochore labelled as path (2). Paths (3) and (4) are isotherms starting from points on the above isochore at $T = 1400$ and 1800°C, while path (5) is chosen so as to maintain the total ionic diffusivity approximately constant.

3. Dissociation of dimers and higher clusters

An important result of our simulation work is the average distribution of clusters in the sample in each given thermodynamic state. A cluster is geometrically defined as a group of

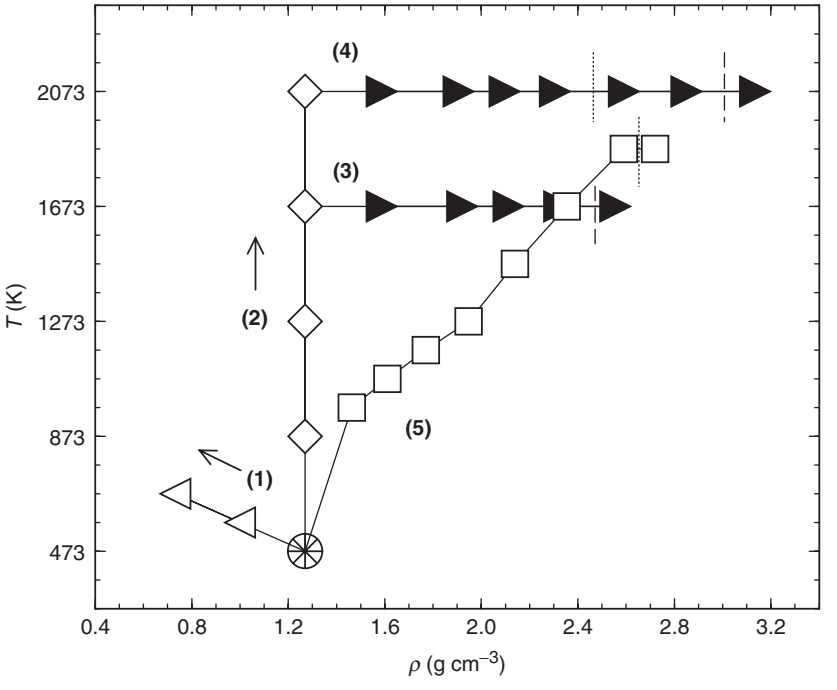

Figure 1. Map of the thermodynamic states studied by simulation in the temperature-density plane (see text; the full lines are guides to the eye). The arrows indicate the paths along which we have only met dissociation of higher molecular clusters into smaller clusters. Vertical lines indicate the approximate locations of the liquid–liquid molecular-to-ionic transition (dotted line) and of the liquid–solid transition (dashed lines).

ions such that all the Al–Cl neighbour distances within the group are < 0.3 nm. We have checked the stability of the cluster population statistics with respect to small variations of such a distance. In the following we report the cluster populations in the form of histograms giving the relative number of various ion groups as a function of the number of ions composing them, as collected during the evolution of the sample after equilibration and averaged over the whole run.

The bottom panel in Figure 2 shows the histogram of cluster populations that we find at the SFP. It is evident that 4-fold ion groups are absolutely dominant and that there are a majority of dimers accompanied by trimers and by some higher clusters. The trimers that we observe are in fact of a chain type formed by attachment of a monomer to a dimer via edge sharing: edge sharing is dominant over corner sharing, which would instead yield trimers in the form of a ring [12]. A similar description applies to the higher clusters, which are again of the chain type and are thus to be envisaged as dynamically connected dimer–monomer or dimer–dimer structures.

The evolution of this initial distribution of clusters along the extrapolated experimental atmospheric pressure isobar that is labelled as (1) in Figure 1 has already been described in the study by Akdeniz *et al*. [12]. Increases in temperature along this path, which lead to a drop in density by almost a factor 2, to dissociation of the higher clusters in favour of dimers and chain trimers, and ultimately establish an equilibrium between the smallest clusters with appearance of a small percentage of monomers.

The other panels in Figure 2 show how the average cluster population evolves away from the SFP along the isochore labelled as (2) in Figure 1. The 4-fold ion groups remain dominant, implying that there is no trace of a MI transition occurring along this isochore in the temperature range that we have explored. There is instead a continuous growth in the population of recognisably separated monomers, which mostly occurs at the expense of the dimer population. The populations of the higher clusters are remarkably stable in this temperature range, but again these are of the chain type, i.e. formed by attachments of lower clusters.

We evaluate the energy required to break a dimer into two monomers as $E \approx 1$ eV. Therefore, we may expect the onset of the dimer-to-monomer transition to start along the isochore at $T \approx 1000$ K according to the empirical rule [26] that a thermally activated excitation process in classical systems may occur at a temperature such that the ratio between the corresponding thermal energy and a characteristic binding energy is of the order 1/10 to 1/20. This crude estimate is clearly consistent with the evolution of the monomer and dimer populations shown in Figure 2. Detachment of an ion from a monomer requires much higher activation energy of several electron volts and should therefore occur along the isochore at much higher temperatures. We can already conclude that compression of the liquid is needed at the temperatures of present interest for the onset of a MI transition, i.e. the MI transition that we study in Section 4 below can be described as due to pressure ionisation. The pressure of the liquid is, of course, also increasing with temperature along the SFP isochore, but we estimate that the isochoric increase of pressure from the SFP to $T = 2073$ K amounts to only 0.6 GPa.

The evolution of cluster populations shown in Figure 2 is accompanied by two remarkable changes in the liquid structure. First of all, the species resolved running coordination numbers, $N_{\alpha\beta}(r)$, defined as:

$$N_{\alpha\beta}(r) = 4\pi n_\beta \int_0^r g_{\alpha\beta}(s) s^2 \mathrm{d}s, \tag{3}$$

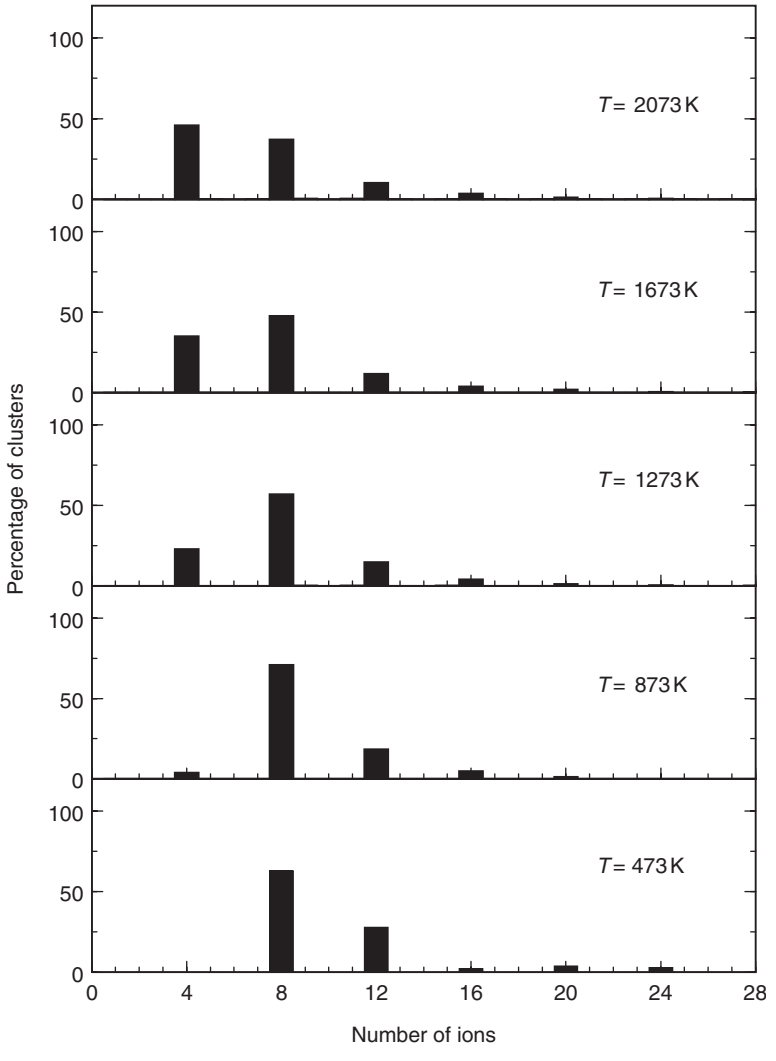

Figure 2. Histograms giving the population of various ion groups in liquid $AlCl_3$ at the indicated temperature along the isochore at density $\rho = 1.27\,\mathrm{g\,cm^{-3}}$.

where a Greek suffix denotes an ionic species, n_β is the mean number density of species b, and $g_{\alpha\beta}(r)$ is the partial distribution function of pairs of ion of species a and b, vary along the isochore (2) in the following manner: (1) a flat plateau in $N_{\mathrm{AlCl}}(r)$ at the value 4 is changing into a slowly rising plateau at a value $\approx$3.5; (2) a broad plateau in $N_{\mathrm{AlAl}}(r)$ at the value 1 evolves into a smooth growth passing at the highest temperature through the value $\approx$0.5 at a value of $\approx$0.35 nm for the Al–Al distance; and (3) $N_{\mathrm{ClCl}}(r)$ remains essentially unchanged. The pair distribution functions in Equation (3) were obtained from the simulation runs by statistical averaging of direct counts of ion pair distances in the sample.

The other remarkable change in liquid structure that we observe along the isochore (2) concerns the change in the state of intermediate range order. We illustrate this

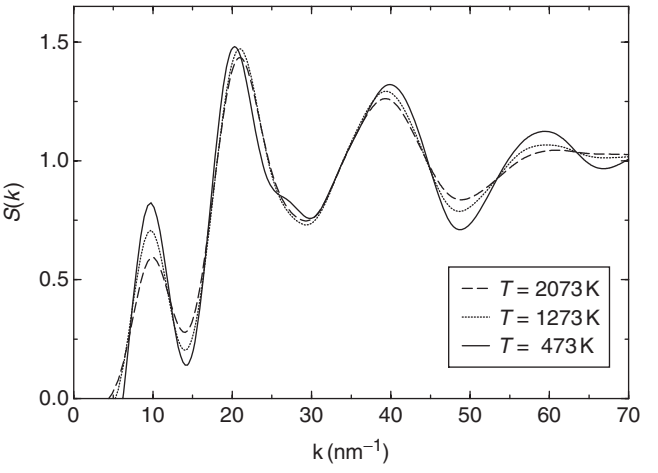

Figure 3. The neutron-weighted structure factor $S(k)$ as a function of wave number k (in nm^{-1}) for liquid $AlCl_3$ along the isochore at density $\rho = 1.27\,\mathrm{g\,cm^{-3}}$, at selected values of the temperature as indicated in the inset.

behaviour by reporting in Figure 3 the neutron-weighted liquid structure factor $S(k)$, defined as

$$S(k) = \frac{b_{\mathrm{Al}}^2 S_{\mathrm{AlAl}}(k) + 6 b_{\mathrm{Al}} b_{\mathrm{Cl}} S_{\mathrm{AlCl}}(k) + 9 b_{\mathrm{Cl}}^2 S_{\mathrm{ClCl}}(k)}{\langle \bar{b} \rangle^2}, \tag{4}$$

where b_α are the coherent neutron scattering lengths [4], $\langle \bar{b} \rangle = b_{\mathrm{Al}} + 3 b_{\mathrm{Cl}}$, and $S_{\alpha\beta}(k)$ are the Faber–Ziman partial structure factors. These we evaluate as $S_{\alpha\beta}(k) = N^{-1} \langle \delta\rho_\alpha(\mathbf{k}) \delta\rho_\beta(-\mathbf{k}) \rangle$, with N the total number of ions and $\delta\rho_\alpha(\mathbf{k})$ the density fluctuation of given wave vector $\mathbf{k}$ for each species. We see from Figure 3 that the pre-peak in $S(k)$ at $k \approx 9.5\,\mathrm{nm^{-1}}$ is progressively reducing as temperature is increased along the isotherm. Breakage of the molecular network and increasing frustration of intermediate range order are thereby indicated. The other main features of the neutron-weighted liquid structure factor show very little change over the whole temperature range. These features reflect correlations mostly between charge-density fluctuation in the peak at $k \approx 21\,\mathrm{nm^{-1}}$ (the 'QQ peak') and correlations between number density fluctuations in the peak at $k \approx 39\,\mathrm{nm^{-1}}$ (the 'NN peak').

4. The MI and liquid–solid transitions

Our next simulation runs start from the two points at temperatures 1673 and 2073 K on the isochore at $\rho = 1.27\,\mathrm{g\,cm^{-3}}$ (corresponding to 0.47 and 0.59 GPa, respectively) and proceed through increases in density along the isotherms marked as (3) and (4) in Figure 1. Some features of the evolution of the system along these two isotherms are similar and do not need separate illustrations, but there is an important difference between them that we shall describe later on in this section. We start by presenting and discussing the observed evolution of the system along the isotherm at $T = 2073\,\mathrm{K}$.

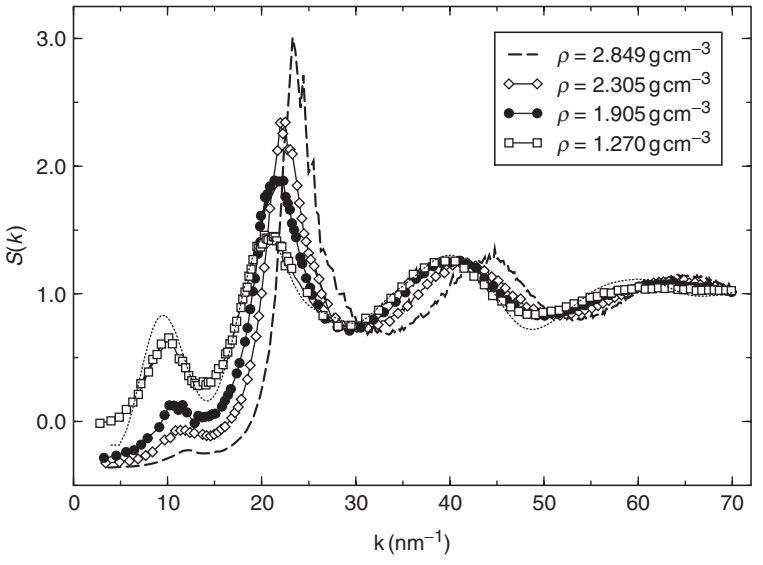

Figure 4. The neutron-weighted structure factor $S(k)$ as a function of wave number k (in nm^{-1}) for liquid $AlCl_3$ along the isotherm at $T = 2073$ K, at selected values of the density ρ as indicated in the inset. The dotted line reports $S(k)$ at the SFP.

We start at this temperature from a liquid containing some majority of monomers (see top panel in Figure 2) and with a reduced degree of intermediate range order, and we can see from Figure 4 that a remarkable evolution is occurring in the QQ peak of the neutron-weighted liquid structure factor as the density is increased along the isotherm. Clearly, the degree of short-range order between charge-density fluctuations is strongly increasing in magnitude. At the same time there is a further progressive reduction in the pre-peak associated with the intermediate range order, and the length scale of all peaks is contracting as one expects from the increase in the average particle density.

The structural evolution of the liquid that accompanies the evolution of $S(k)$ shown in Figure 4 is further illustrated for the same isotherm in Figures 5 and 6. Figure 5 shows the behaviour of the running partial coordination numbers: in particular we see that at the highest density, which refers to the crystal, the Al–Cl coordination number approaches a value of $\approx$6 as it passes through the first neighbour bond length. A most clear signal of the structural change that has occurred along the isotherm is given by the data in Figure 6, showing the statistics of average cluster populations. It is seen that at a density $\rho \approx 2.30$ g cm^{-3} two different types of cluster populations start coexisting: one mostly consists of monomers and dimers, and the other consists of clusters having essentially the size of the simulation sample. On further increases in density the former population type disappears and the latter acquires a single size, which is equal to the sample size. Solidification is met at still higher density and is confirmed by the study of the mean square ionic displacements, as will be reported in the next section.

To summarise the results of this part of our study, on increasing the density of the simulation sample along the isotherm at $T = 2073$ K we meet first a structural change from a molecular liquid to a dissociated ionic liquid, and then solidification into a 6-fold coordinated crystal. We also remark that the MI liquid transition that we observe on this

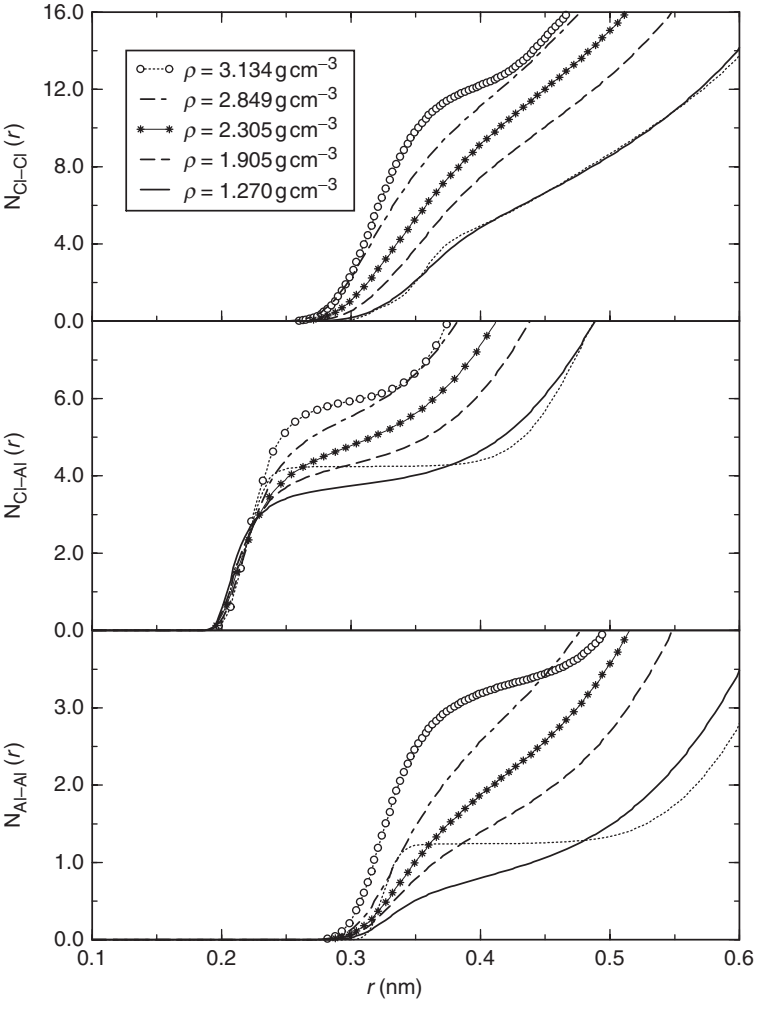

Figure 5. Running coordination numbers $N_{\alpha\beta}(r)$ as functions of ion pair distance r (in nm) for $AlCl_3$ along the isotherm at $T = 2073$ K, at selected values of the density ρ as indicated in the inset. The dotted lines report $N_{\alpha\beta}(r)$ at the SFP.

isotherm is far from sharp, since it is spread over a range of density from 2.3 to 2.6 g cm^{-3} approximately, corresponding to pressures from 6.4 to 10.1 GPa.

The behaviour that we observe in our simulation runs along the isotherm at $T = 1673$ K is again of a similar type for what concerns the properties shown in Figures 4, 5 and 6, but here the locations of the MI transition and of the solidification transition coincide, as far as we can tell from our runs. We interpret this result as reflecting the presence of some anomaly on the melting curve: the higher isotherm appears to meet the melting curve above the anomaly and the lower isotherm appears to meet it below the anomaly, with the anomaly being due, as in the observations of Brazhkin *et al.* [13,14], to the branching out of the MI transition away from the melting curve. The location of these transitions is shown in Figure 1 by vertical lines. We estimate that the pressure in the simulation sample increases by about 8 GPa along the lower isotherm before solidification occurs, and along

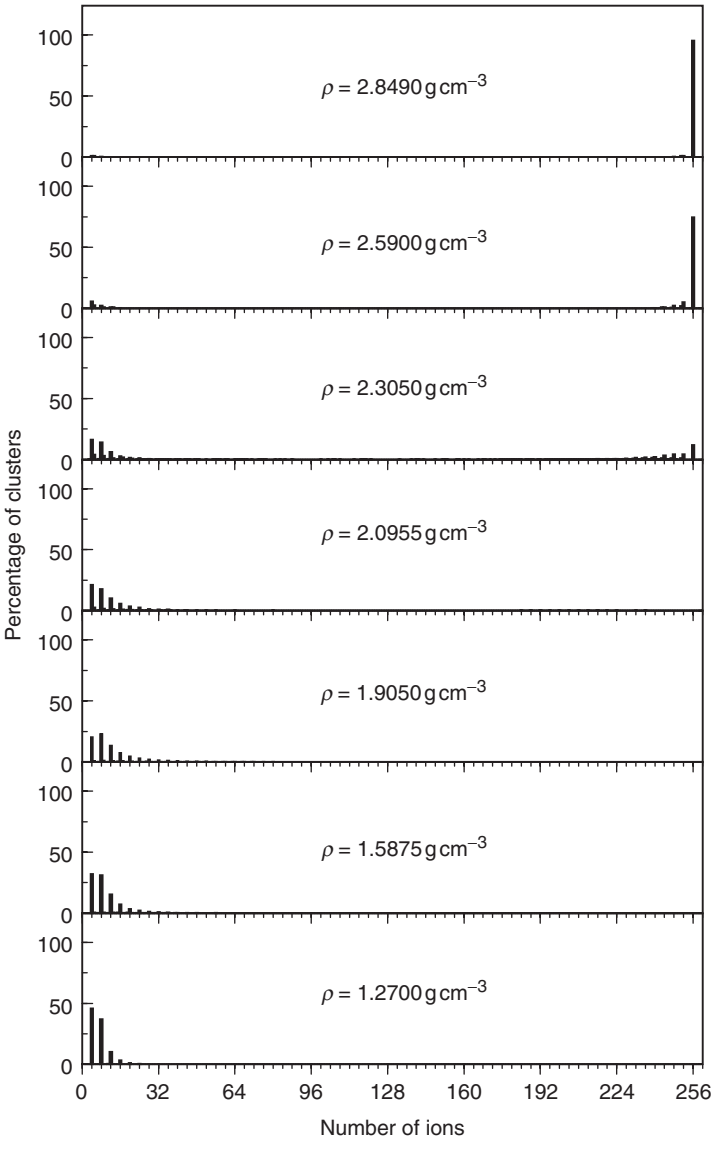

Figure 6. Histograms giving the population of various ion groups in $AlCl_3$ along the isotherm at $T = 2073$ K, at selected values of the density ρ as indicated$_\omega$.

the higher one by about 10 GPa before the onset of the MI transition in the liquid, and by a further 9 GPa before solidification.

The next question that we may ask is what is the structure of the crystal that is formed on solidification? On both isotherms we find that this is the same as the experimentally observed structure of the $AlCl_3$ crystal at the SFP [2]: that is, a layer structure in which the chlorines form a distorted close-packed sub-lattice sandwiching in alternate layers the Al ions in 6-fold coordination sites. Figure 7 reports this crystal structure as we found it in the isothermal run at $T = 1673$ K.

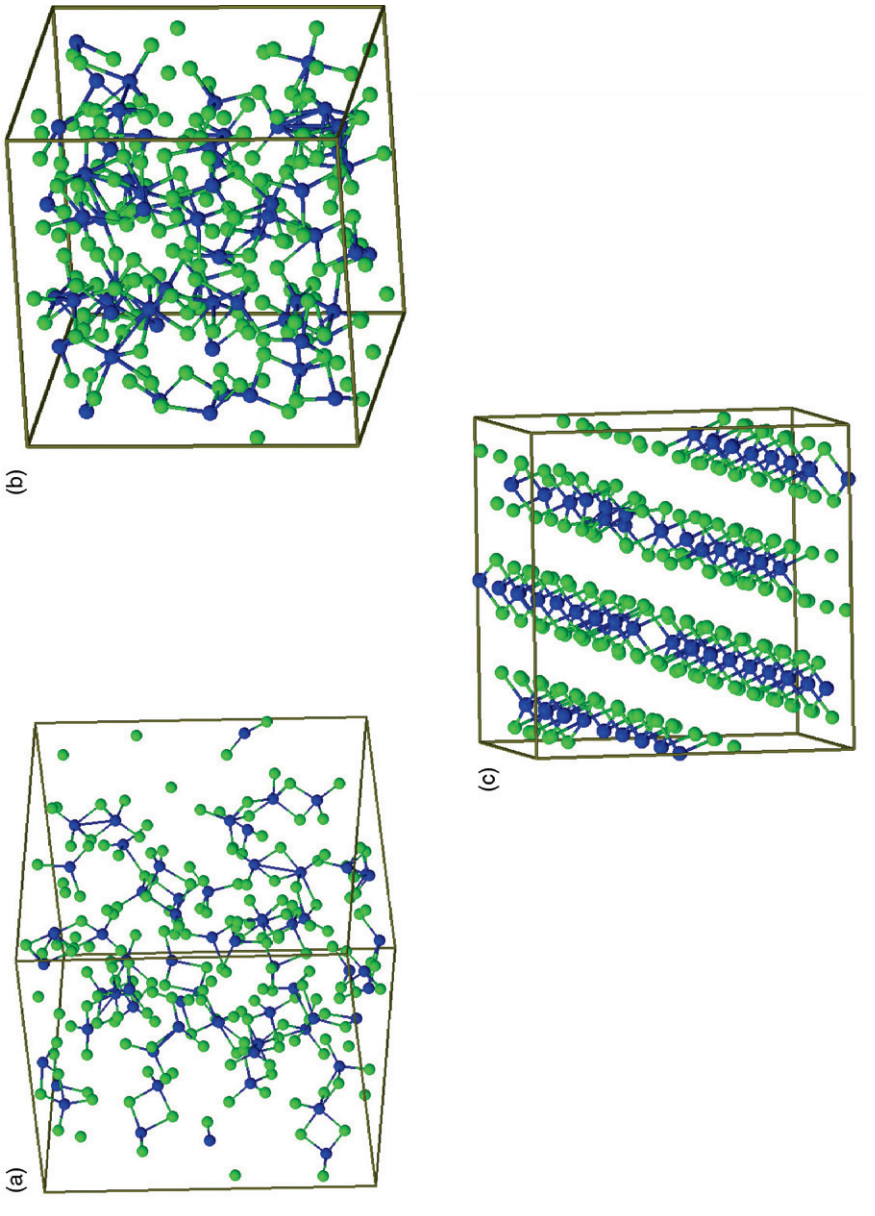

Figure 7. Snapshots of the structure of the simulation sample (a) in the molecular liquid state at $T = 473$ K and $\rho = 1.27\,\mathrm{g\,cm^{-3}}$ (top left), (b) in the ionic liquid state at $T = 2073$ K and $\rho = 2.849\,\mathrm{g\,cm^{-3}}$ (top right) and (c) after solidification at $T = 1673$ K and $\rho = 2.555\,\mathrm{g\,cm^{-3}}$ (bottom). The edges of the cubic simulation box have been drawn. Bonds between atoms of the simulation box and periodic images in the neighbour cells have not been shown.

5. The role of ionic diffusivity

We report in this section, simulational results regarding the velocity autocorrelation functions (VACF) and the mean square displacements (MSD) of the ions in a variety of thermodynamic states. The self-diffusion coefficients of the ions are then obtained from their MSD through the Einstein relation.

We first report in Figure 8 the spectrum $C_v(\omega)$ of the total VACF of the melt (1) at the SFP, (2) at $T = 2073$ K on the SFP isochore; and (3) at density $\rho = 2.59\,\mathrm{g\,cm^{-3}}$ after the MI transition has occurred on the isotherm at $T = 2073$ K. The spectrum at the SFP contains a number of rather sharp features, which can be put into correspondence with the vibrational spectrum of the isolated Al_2Cl_6 dimer: the vibrational frequencies of the dimer as calculated in the harmonic approximation are indicated by upward-pointing arrows on the horizontal axis, over a frequency range extending up to almost $300\,\mathrm{cm^{-1}}$ for the bending modes and from $300\,\mathrm{cm^{-1}}$ to about $760\,\mathrm{cm^{-1}}$ for the stretching modes. There are also, in this spectrum, traces of vibrational frequencies associated with the chain trimer: these are the two small peaks at $\approx 240\,\mathrm{cm^{-1}}$ and near $700\,\mathrm{cm^{-1}}$ as indicated by the two downward-pointing arrows.

Isochoric heating of the melt up to $T = 2073$ K broadens out all spectral features, but still leaves three main broad peaks corresponding to the lowest and intermediate bending modes and to the highest stretching modes. The VACF spectrum in the ionic liquid has instead a completely different shape: it contains a very broad peak in the region of the bending modes of the dimer and a smooth drop through the hydrodynamic plasma frequency. In fact this spectrum resembles the spectrum of long-wavelength charge-density fluctuations in a typical liquid like NaCl [27], except that the zero-frequency peak reflecting DC ionic conductivity in the latter spectrum is missing because of the finiteness of the simulation sample.

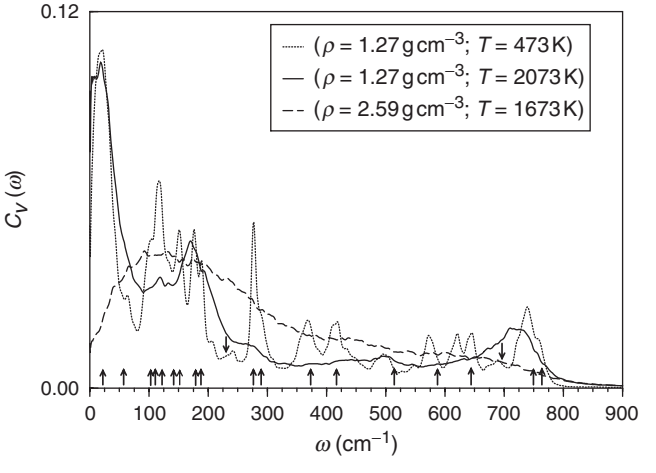

Figure 8. The spectrum $C_v(\omega)$ of the total velocity autocorrelation function as a function of frequency ω (in $\mathrm{cm^{-1}}$) for liquid $AlCl_3$ in the three thermodynamic states indicated in the inset. The arrows on the horizontal axis indicated the harmonic vibrational frequencies of the Al_2Cl_6 dimer. The two downward-pointing arrows indicated traces of the vibrational frequencies of the Al_3Cl_9 chain trimer in the SFP spectrum.

Figure 9 reports the MSD of the two ionic species as functions of time for various values of the density along the isotherm at $T = 2073$ K. From the asymptotic slope of these data and of similar data along the other isotherm we have obtained the values of the self-diffusion coefficients that are reported in Table 1.

It is seen from these data that at the density of the SFP the two species diffuse at reasonable and very similar rates, consistently with an essentially molecular structure of the melt. The diffusivity of the halogens is slightly higher than that of the Al species at this density and at a series of higher values of the density, but with the onset of the MI liquid–liquid transition along the higher isotherm the two diffusivities become practically identical and indeed invert their order at still higher densities. Thus also mass transport can provide a clear signal of the transition in the bonding character in the liquid state. Finally, the diffusivities are seen to almost vanish for both species after solidification.

In view of the role that is apparently being played by mass transport in the liquid–liquid transition we have carried out some further simulation runs along the path that is labelled as (5) in Figure 1. Along this path we simultaneously vary the temperature and the density so as to keep approximately constant the total diffusivity. In practice this procedure suppresses the inversion of the diffusivities of the two species, although they become practically identical at the highest densities, and this is obviously not favourable to solidification. We nevertheless meet the MI transition also along this path, as is indicated by the shape of the running coordination numbers shown in Figure 10.

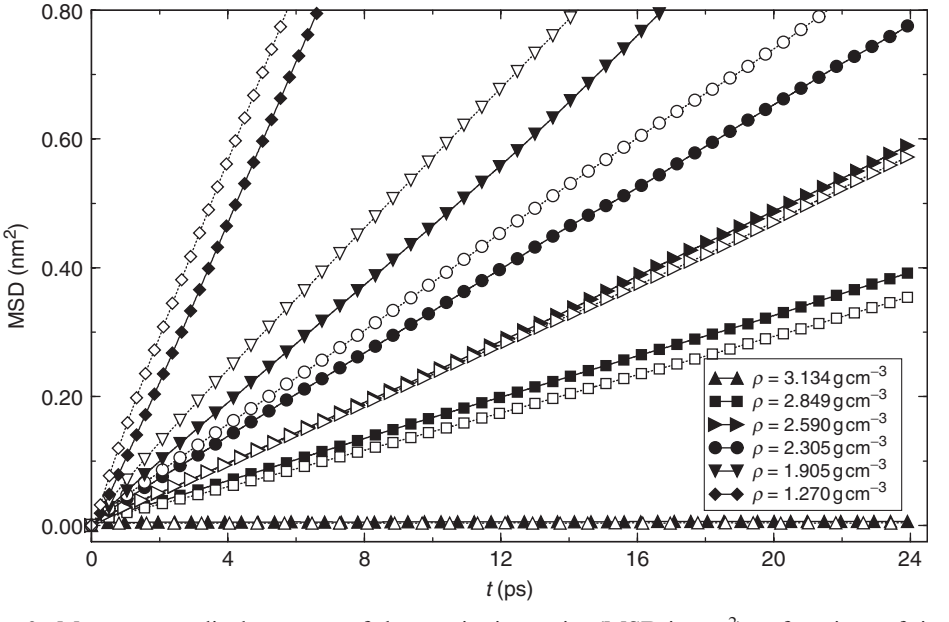

Figure 9. Mean square displacements of the two ionic species (MSD in nm^2) as functions of time t (in picoseconds) in $AlCl_3$ at $T = 2073$ K and various values of the density as shown in the inset. The top pair of curves refers to the density of the SFP and the lowest pair refers to the solid. Open symbols: Cl, filled symbols: Al.

Table 1. Self-diffusion coefficients D_α of the two ionic species in $AlCl_3$ (in $10^{-5}\,cm^2\,s^{-1}$) at selected values of the density ρ (in $g\,cm^{-3}$) along the isotherms at temperatures 1673 K and 2073 K.

$T = 1673$ K									
ρ	1.27	1.5875	1.92	2.112	2.323	2.439	2.5	2.53	2.555
D_{Al}	15.4	10.0	5.01	3.93	3.03	2.22	1.71	1.27	0.0012
D_{Cl}	16.0	11.2	6.22	4.85	3.37	2.74	2.10	1.53	0.0011
$T = 2073$ K									
ρ	1.27	1.5875	1.905	2.0955	2.305	2.59	2.849	3.134	
D_{Al}	20.8	11.9	8.13	7.95	5.36	4.07	2.68	0.011	
D_{Cl}	22.3	13.6	9.14	8.31	6.12	3.92	2.43	0.016	

6. Summary and future perspectives

In summary, we have presented results from molecular dynamic simulation of the structure and the diffusive motions in a model for $AlCl_3$ over broad ranges of temperature and density, using an interionic force law that was determined from properties of molecular monomers and dimers in the gaseous phase, as described in terms of the interactions between the individual component ions. This force law has been previously shown [11] to yield a good quantitative account of the neutron-weighted structure factor of the liquid phase of this and other related compounds near the SFP. Our simulation runs have traced the properties of the liquid along several paths in the temperature-density plane and have thereby demonstrated the following structural transitions: (1) dissociation of molecular clusters towards a liquid of molecular monomers on increasing temperature along the isochore passing through the SFP; (2) change in bonding character from molecular to ionic, followed by crystallisation of a dissociated ionic liquid, on increasing density along a high-temperature isotherm; and (3) change in ionic character from MI, in coincidence with crystallisation, on increasing density along a lower temperature isotherm. The scenario that emerges from these results is consistent with the observations reported by Brazhkin *et al.* [13,14] from X-ray diffraction experiments on $AlCl_3$ at high pressure and temperature.

We have tested the reliability of the model to its ingredients by carrying out parallel simulation runs using modifications of the interionic force law consisting in (1) replacement of nominal ionic charges by fractional charges adjusted to measured vibrational frequencies of the isolated clusters [23]; or (2) suppression of the van der Waals interactions between the halogens. These tests confirm the basic scenario of liquid–liquid and liquid–solid transitions that we have summarised just above, but also show that the quantitative details are model dependent. In particular, both these changes in the interionic force law tend to diminish the cohesion of the molecular clusters and thus tend to shift to a lower temperature the branching-off of the MI transition away from the solidification transition. Thus, while we cannot trust the quantitative details of our results concerning the thermodynamics of the structural transitions, we have nevertheless presented estimates of the pressure to indicate that the transition that we have reported upon occur in similar ranges of temperature and pressure as in the real $AlCl_3$ material studied by Brazhkin *et al.* [13]. Resorting to expensive computer quantum mechanical methods may ultimately ensure full contact between theory and experiment.

With regard to future developments, two main perspectives immediately suggest themselves. First, there is certainly scope for refinements of the interionic force model on

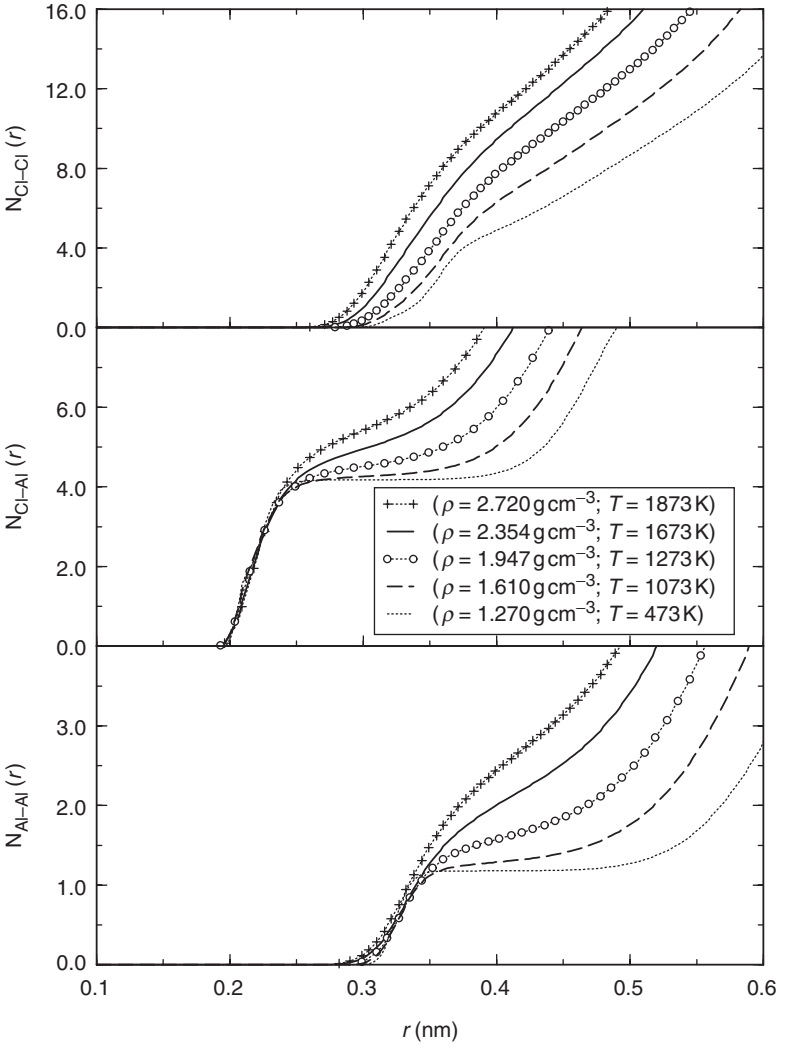

Figure 10. Running coordination numbers $N_{\alpha\beta}(r)$ as functions of ion pair distance r (in nm) for $AlCl_3$ along the 'isodiffusivity' path (5) (Figure 1), at the values of temperature and density shown in the inset. The dotted curves refer to the SFP.

the basis of studies of the equation of state of this and similar materials in both the vapour and the liquid phase. Second, our study of transport in the liquid phase should be extended to other properties such as the DC ionic conductivity and the deviations from the Nernst–Einstein relation, which would directly reflect the correlated motions of the two ionic species.

Acknowledgements

M.P.T. thanks Prof. V.E. Kratsov and the Condensed Matter and Statistical Physics Section of the Abdus Salam International Center for Theoretical Physics in Trieste for their hospitality.

References

[1] M.P. Tosi, D.L. Price, and M.-L. Saboungi, Annu. Rev. Phys. Chem. **44**, 173 (1998).
[2] R.W.G. Wyckoff, *Crystal Structures*, Vol 2 (Interscience, New York, 1964).
[3] Z. Akdeniz and M.P. Tosi, Proc. R. Soc. **A437**, 85 (1992).
[4] Y.S. Badyal, D.A. Allen, and R.A. Howe, J. Phys. Condens. Matter **6**, 10193 (1994).
[5] R.L. Harris, R.E. Wood, and H.L. Ritter, J. Am. Chem. Soc. **73**, 3150 (1951).
[6] M.-L. Saboungi, M.A. Howe, and D.L. Price, Mol. Phys. **79**, 847 (1993).
[7] P.S. Salmon, Proc. R. Soc. **A445**, 351 (1999).
[8] B. Kirchner, A.P. Seitsonen, and J. Hutter, J. Phys. Chem. **B110**, 11475 (2006).
[9] A.L.L. East and J. Hafner, J. Phys. Chem. **B111**, 5316 (2007).
[10] F. Hutchinson, M.K. Walters, A.J. Rowley, and P.A. Madden, J. Chem. Phys. **110**, 5821 (1999).
[11] R. Ruberto, G. Pastore, A. Akdeniz, and M.P. Tosi, Mol. Phys. **105**, 2383 (2007).
[12] Z. Akdeniz, Z. Çiçek Önem, R. Ruberto, G. Pastore, and M.P. Tosi. *Phys. Chem. Liq.*, **46,** 1 (2008).
[13] V.V. Brazhkin, Y. Katayama, A.G. Lyapin, S.V. Popova, Y. Inamura, H. Saitoh, and W. Utsumi, JETP Lett. **82**, 713 (2005).
[14] V.V. Brazhkin, A.G. Lyapin, S.V. Popova, Y. Katayama, H. Saitoh, and W. Utsumi, J. Phys. Condens. Matter **19**, 246104 (2007).
[15] D. Saumon and G. Chabrier, *Phys. Rev.* **A46**, 2084 (1992).
[16] W.R. Magro, D.M. Ceperley, C. Pierleoni, and B. Bernu, Phys. Rev. Lett. **76**, 1240 (1196).
[17] Z. Akdeniz, G. Pastore, and M.P. Tosi, Nuovo Cimento **20D**, 595 (1998).
[18] A. Karaman, Z. Akdeniz, and M.P. Tosi, Phys. Chem. Liq. **44**, 353 (2006).
[19] G. Csanyi, T. Albaret, M.C. Payne, and A. DeVita, Phys. Rev. Lett. **93**, 175503 (2004).
[20] F. Tangney and S. Scandolo, J. Chem. Phys. **56**, 9673 (2003).
[21] W.R. Busing, Trans. Am. Crystallogr. Ass. **6**, 57 (1970).
[22] A.R. Cochran, Crit. Rev. Solid State Sci. **2**, 1 (1971).
[23] Z. Akdeniz and M.P. Tosi, Z. Naturforsch. **54a**, 180 (1999).
[24] M.P. Allen and D.J. Tildesley, *Computer Simulation of Liquids* (Oxford University Press, New York, 1987).
[25] G.J. Janz, J. Phys. Chem. Ref. Data **17**, 1 (1988).
[26] N.H. March and M.P. Tosi, Phys. Chem. Liq. **10**, 39 (1980).
[27] D.K. Chaturvedi, U. Marini Bettolo Marconi, and M.P. Tosi, Nuovo Cimento **B57**, 319 (1980).